

Outstanding nonlinear optical properties of methylammonium- and Cs-PbX₃ (X = Br, I, and Br-I) perovskites: Polycrystalline thin films and nanoparticles ^{EP}

Cite as: APL Mater. 7, 041106 (2019); <https://doi.org/10.1063/1.5090926>

Submitted: 31 January 2019 . Accepted: 20 March 2019 . Published Online: 05 April 2019

Isaac Suárez ^{ID}, Marta Vallés-Pelarda ^{ID}, Andrés F. Gualdrón-Reyes ^{ID}, Iván Mora-Seró ^{ID}, A. Ferrando, Humberto Michinel, José Ramón Salgueiro, and Juan P. Martínez Pastor ^{ID}

COLLECTIONS

^{EP} This paper was selected as an Editor's Pick



View Online



Export Citation



CrossMark



Measure Ready
M91 FastHall™ Controller

A revolutionary new instrument
for complete Hall analysis

Lake Shore
CRYOTRONICS

Outstanding nonlinear optical properties of methylammonium- and Cs-PbX₃ (X = Br, I, and Br-I) perovskites: Polycrystalline thin films and nanoparticles

Cite as: APL Mater. 7, 041106 (2019); doi: 10.1063/1.5090926

Submitted: 31 January 2019 • Accepted: 20 March 2019 •

Published Online: 5 April 2019








View Online



Export Citation



CrossMark

Isaac Suárez,^{1,2,a)}  Marta Vallés-Pelarda,³  Andrés F. Gualdrón-Reyes,^{3,4,5}  Iván Mora-Seró,³  A. Ferrando,⁶ Humberto Michinel,⁷ José Ramón Salgueiro,⁷ and Juan P. Martínez Pastor^{1,a)} 

AFFILIATIONS

¹UMDO, Instituto de Ciencia de los Materiales, Universidad de Valencia, Valencia 46071, Spain

²Escuela Técnica Superior de Ingenieros de Telecomunicación, Universidad Rey Juan Carlos, 28943 Madrid, Spain

³Institute of Advanced Materials (INAM), Universitat Jaume I, Av. Sos Baynat, s/n, 12071 Castelló, Spain

⁴Centro de Investigaciones en Catálisis (CICAT), Universidad Industrial de Santander, Piedecuesta, Santander C.P. 681011, Colombia

⁵Centro de Investigación Científica y Tecnológica en Materiales y Nanociencias (CMN), Universidad Industrial de Santander, Piedecuesta, Santander C.P. 681011, Colombia

⁶Departament d'Òptica i Optometria i Ciències de la Visió, Universitat de València, Dr. Moliner, 50, Burjassot, 46100 Valencia, Spain

⁷Escola de Enxeñaría Aeronáutica e do Espazo, Universidade de Vigo, Campus As Lagoas, 32004 Ourense, Spain

^{a)}isaac.suarez@uv.es and juan.mtnez.pastor@uv.es

ABSTRACT

Metal Halide Perovskites (MHPs) have arisen as promising materials to construct cost-effective photovoltaic and light emission devices. The study of nonlinear optical properties of MHPs is necessary to get similar success in nonlinear photonic devices, which is practically absent in the literature. The determination of the third order nonlinear coefficients is typically done by the Z-scan technique, which is limited by the scattering of polycrystalline thin films. In this work, we have studied nonlinear optical properties of polycrystalline CH₃NH₃PbX₃ (MAPbX₃) thin films and colloidal CsPbX₃ nanoparticles with three different bandgaps (X₃ = I₃, Br₃, and Br_{1.5}I_{1.5}). Their bright generation of photoluminescence under infrared illumination demonstrates an excellent efficiency of multiphoton absorption. The nonlinear absorption coefficient (β) was studied by analyzing the transmitted light through the samples, observing the expected E_g^{-3} dependence with values as high as $\beta = 1500$ cm²/GW. In addition, we proposed the use of a modified Z-scan technique with imaging processing to analyze the nonlinear refraction coefficient (n_2) under the laser damage threshold. Our experimental data agree quite well with theoretical predictions, demonstrating the accuracy of the method and potential applications to other thin films. Moreover, n_2 parameter reaches values of 3.5 cm²/GW, indicating the suitability of MHPs for nonlinear photonics.

© 2019 Author(s). All article content, except where otherwise noted, is licensed under a Creative Commons Attribution (CC BY) license (<http://creativecommons.org/licenses/by/4.0/>). <https://doi.org/10.1063/1.5090926>

In the last years, organic-inorganic and inorganic Metal Halide Perovskites (MHPs) have demonstrated extraordinary capabilities to develop high quality optoelectronic devices under a cheap and straightforward technology.^{1,2} MHPs are direct bandgap semiconductors that can be synthesized by low-cost and trouble-free

solution process techniques in polycrystalline thin films^{3,4} or nanoparticles (NPs)^{5,6} with the general chemical formula of perovskites ABX₃,⁴ where the cation A is usually fixed as organic [i.e., methylammonium (MA), CH₃NH₃⁺] or inorganic (cesium cation, Cs⁺), B is a metal (usually Pb), and X a halide (Cl⁻, Br⁻, and I⁻).

MHP materials have reached special attention in photovoltaics due to their sharp and strong absorption edge, large carrier diffusion lengths, and relatively small non-radiative recombination rates. Nowadays, conversion efficiencies of perovskite solar cells surpass 23%.⁷ In addition, these materials turn out to be an excellent active medium for generation and amplification of light⁸ because of their high efficiency of emission at room temperature and tunable bandgap.⁹ Consequently, MHPs have successfully been applied in light emitting diodes,¹⁰ optical amplifiers,^{10,11} or lasers.¹² Indeed, the current technology advances with MHP materials allow the integration of amplification/photodetection functionalities¹³ and also patterning of different nanophotonic components.¹⁴ Thus, since there is an increasing role of MHPs in photonics technology, next step is the use of their nonlinear optical properties for other potential applications and devices, such as switching, data storage, supercontinuum generation, optical limiting, or frequency combs.¹⁵ This would be possible if the nonlinear optical properties of MHPs meet several requirements, as defined below.

Semiconductors are usually centrosymmetric materials where the optical nonlinearities depend on the third order susceptibility ($\chi^{(3)}$). This magnitude is a complex number, where the real part is proportional to the nonlinear refractive index (n_2) and the imaginary part to the nonlinear absorption (β_2). In these conditions, the complex refractive index, n , will be modified with the incident intensity of light (I) according to

$$\Delta n = n_2 \cdot I - i \cdot \frac{\lambda}{4 \cdot \pi} \cdot \beta_2 \cdot I, \quad (1)$$

where λ is the wavelength of the incident light. The nonlinearity derived from n_2 is called Kerr effect and it is related with beam focusing and harmonic generation, while β_2 is responsible for the two-photon absorption (2PA) mechanism. Since both parameters are intrinsically interconnected by Kramers-Kronig relationships, their coexistence limits the efficiency of each particular nonlinear effect. From a practical point of view, the following figure of merit, namely, *FOM*, measures the suitability of a material for a given application¹⁶

$$FOM = \frac{1}{\lambda} \cdot \frac{n_2}{\beta_2}. \quad (2)$$

The most popular method to characterize the above defined nonlinear optical parameters, n_2 and β_2 , is the well-known Z-scan technique.¹⁷ This technique consists of translating the sample along the propagation direction (z), the Z-axis, in such a way that the diameter of the laser beam spot on the sample, and thus its intensity, can be gradually modified with the sample position by using a focusing lens. Using this simple mechanism, n_2 can be determined by measuring the far field distribution of the focusing and defocusing beam as a function of z , while β_2 is obtained by the attenuation of the light at the highest excitation fluency.

Consequently, nonlinear optical parameters of a broad range of semiconductors have been measured using the Z-scan technique. These parameters follow a universal variation predicted by a (parabolic) two-band model.¹⁸ Particularly, n_2 and β_2 can be scaled down with the bandgap (E_g) following a E_g^{-4} and E_g^{-3} dependence, respectively.^{18,19} As one would expect, Z-scan has been also applied to characterize different MHP materials in different papers,

separately, as MAPbBr₃ and CsPbX₃ nanocrystals in colloidal solution,^{20,21} MAPbI₃ polycrystalline thin films,^{22–24} or thin films prepared with CsPbBr₃ nanocrystals.²⁵ Nevertheless, the experimental values reported in the above referred publications reveal a strong dispersion and, in most cases, do not follow the dependence on E_g predicted by the two-band model theory, as pointed out in our recent perspective paper.²⁶ These discrepancies could arise from the limitations of the Z-scan technique applied to polycrystalline thin films of MHPs, where the scattering (or even damage under high incident laser power) through the submicron-size grains can lead to an overestimation of the nonlinear parameters. Indeed, an alternative characterization of β preferred by some authors consists of measuring the transmittance of a focused laser beam through the nonlinear material. Since this method is not seriously affected by light scattering, it provides a more accurate value for the nonlinear absorption coefficient. For example, this technique revealed $\beta_2 = 5$ cm/GW in CsPbBr₃ monocrystals,²⁷ $\beta_2 = 15–21$ cm/GW with the right E_g^{-3} dependence in quasi-2D MHP films,²⁸ or a giant $\beta_2 = 2 \times 10^5$ cm/GW in MHP flakes.²⁹ Therefore, the efficiency of nonlinear absorption in MHP materials would turn out to be equal or greater (up to a factor five) than in other semiconductors, such as CdSe/ZnS or CdTe colloidal quantum dots, silicon, or MoX₂ (X = S, Se, and Te).^{26,29} Demonstrated applications of nonlinear optical materials include up-conversion lasing under infrared excitation^{30,31} or saturable absorbers for ultrafast pulse generation.³² In the same way, n_2 can be also characterized by analyzing the intensity of third harmonic generation or four wave mixing as a function of the excitation fluency.^{28,33} However, this alternative method only provides an indirect estimation of the Kerr effect and requires the comparison with a reference nonlinear material. In addition, the characterization of n_2 in MHPs is usually performed under picosecond (ps) or femtosecond (fs) pulses to avoid thermal effects, although longer pulses or even Continuous Wave (CW) excitation would be desirable in practical applications.

In this work, we have tried to reach representative values for nonlinear optical parameters of several MHP materials under nanosecond (ns) pulsed laser excitation. Furthermore, these MHPs were prepared under similar conditions in the form of polycrystalline thin films and NPs (both in colloidal solution and forming solid thin films) and with different bandgap energies, but within the same material family: MAPbX₃ and CsPbX₃ (X₃ = I₃, Br₃, and Br_{1.5}I_{1.5}). In this way, we can also infer if the nonlinear optical parameters that are reported in the present paper are consistent with the scaling law for semiconductors. From the point of view of the optical characterization, we have used three different experimental methods to reveal and/or determine the nonlinear optical parameters of MHPs: photoluminescence (PL) under 2 or 3 photon absorption processes, transmittance through the materials of a focused laser beam, and a modified Z-scan method. In the latter case, the laser beam shape is recorded by a CCD camera as a function of Z, from which both intensity and laser beam waist can be analyzed. Our results demonstrate that scattering of the polycrystalline film can be avoided by (i) Fast Fourier Transform (FFT) and filtering of the image and (ii) a right comparison of the spot under high and low excitation fluencies. Furthermore, the real time observation of the laser beam transmittance through the sample enables us to limit laser power below the limit over which deterioration of

the film occurred. Our results are consistent with the expected E_g^{-4} and E_g^{-3} dependences for semiconductors with values of n_2 and β_2 up to $3.5 \text{ cm}^2/\text{GW}$ and $1500 \text{ cm}/\text{GW}$, indicating the suitability of MHP materials for nonlinear optics.

MPbX₃ films were prepared in ambient conditions on a commercial borosilicate substrate. First, a $\approx 40 \text{ nm}$ layer of TiO₂ was deposited by spray-pyrolysis at 450°C using titanium diisopropoxide bis(acetylacetonate) (Sigma-Aldrich, 75% in isopropanol) diluted in ethanol (PanReac AppliChem, 99.8%) (1:9) and O₂ as carrier gas. Then, MPbX₃ films were deposited by spin-coating the corresponding perovskite solutions at 4000 rpm for 50 s and annealed for 3 min at 100°C . After deposition, the thickness of the films was around 250 nm.

For the perovskite solution preparation, the corresponding lead salts, PbI₂ (TCI, 99.99%) and PbBr₂ (TCI, 99.99%), and methylammonium salts, MAI and MABr (Greatcell Solar), were mixed to obtain 1.35M perovskite solutions using *N,N*-dimethylformamide (Sigma-Aldrich, 99.8%) as solvent. For MPbI₃ films, 7% of dimethyl sulfoxide (Sigma-Aldrich, 99.9%) was added and diethyl ether (Sigma-Aldrich, 99.0%) was used as antisolvent.

CsPbX₃ NPs were synthesized following the hot-injection method described by Kovalenko and co-workers, with some modifications.³⁴ All the reactants were used as received without an additional purification process. Briefly, a Cs-oleate solution was prepared by mixing 0.41 g Cs₂CO₃ (Sigma-Aldrich, 99.9%), 1.25 ml of oleic acid (OA, Sigma Aldrich, 90%), and 20 ml of 1-octadecene (1-ODE, Sigma-Aldrich, 90%) into a 50 ml-three neck flask at 120°C under vacuum for 1 h with constant stirring. Then, the mixture was N₂-purged and heated at 150°C until the Cs₂CO₃ was completely dissolved. The solution was stored under N₂, maintaining the temperature at 100°C to prevent the Cs-oleate oxidation.

For the synthesis of CsPbBr₃, CsPbI₃, and CsPbBr_{1.5}I_{1.5} NPs, 0.69 g PbBr₂ (ABCR, 99.999%), 0.87 g PbI₂ (TCI, 99.99%), or the corresponding PbBr₂/PbI₂ mixture were mixed with 50 ml of 1-ODE in a 100 ml-three neck flask. The mixture was heated at 120°C under vacuum for 1 h, with constant stirring. Then, 5 ml of both OA and oleylamine (OLA, Sigma-Aldrich, 98%) were separately added to the flask under N₂ and rapidly heated to reach 170°C , injecting quickly 4 ml of Cs-oleate solution. Finally, the flask was immersed into a bath ice for 5 s to quench the reaction mixture.

For the isolation of perovskite NPs, the colloidal solutions were centrifuged at 4700 rpm for 10 min. The NPs pellets were separated after discarding the supernatant and redispersed in hexane to

prepare a concentration of 50 mg ml^{-1} . For optical characterization purposes, NPs were dropped in a 1 mm quartz cuvette in a fixed concentration of 5 mg/ml.

A commercial NanoCalc-2000 reflectometer (Mikropack) was used to measure absorption spectra in MPbX₃ films deposited on borosilicate substrates. Absorption of CsPbX₃ colloids was characterized by analyzing the transmittance spectra of a halogen lamp with a USB650 Ocean Optics spectrometer.

Photoluminescence (PL) measurements on MPbX₃ films were registered in backscattering geometry by using a continuous wave (CW) excitation laser at 404 nm under a weak pump fluency of $20 \text{ W}/\text{cm}^2$ and collecting the back-emitted PL into a USB650 Ocean Optics spectrometer. PL under two photon absorption was characterized by illuminating the sample with a 1064 nm Nd:Yag laser (1 ns, 20 kHz) with a variable excitation fluency up to $1 \text{ GW}/\text{cm}^2$. The same lasers and spectrometer were used to measure PL in the CsPbX₃ colloids in a quartz cuvette.

Nonlinear characterization of samples was carried out by illuminating the samples with a 1064 nm Nd:Yag laser (1 ns, 20 kHz). Nonlinear absorption coefficient was measured by studying the transmittance through the sample as a function of the excitation fluency (I) ranged between 0.05 and $1 \text{ GW}/\text{cm}^2$ with neutral density filters. Nonlinear refraction coefficient was analyzed in the Z-scan geometry shown in Fig. 1. In MPbX₃ films, the excitation beam was first focused into $11\text{--}13 \mu\text{m}$ spot with the aid of a 25 mm focal lens. In the case of CsPbX₃ nanocrystals, the beam was focused in $36\text{--}40 \mu\text{m}$ spot with a 75 mm focal lens. In both cases, the Rayleigh length ($357 \mu\text{m}$ and 3.8 mm for films and colloidal solution, respectively) is longer than the thickness of the sample or cuvette to fulfill the thin sample approximation condition. Then, the light transmitted through the film or cuvette was collected with a 100 mm focal lens to a Thorlabs CCD DCU224M while the sample is translated with a Thorlabs MTS25A-Z8 platform. The camera recorded one image for each translation step.

Optical absorption and PL spectra of MAPbX₃ films and CsPbX₃ colloidal solutions are tuned with the halide composition (X) due to the different bandgap in each material (see Fig. 1 and Table I). Absorption in MAPbX₃ films [solid lines in Fig. 1(a)] shows a sharp edge at 2.37–2.40, 1.83–1.87, and 1.60–1.66 eV for X₃ = Br₃ (green), X₃ = Br_{1.5}I_{1.5} (orange), and X = I₃ (red), respectively, in agreement with previous publications.³⁵ The absorption coefficient becomes negligible below those band edges, while it reaches values higher than 10^5 cm^{-1} when they are illuminated at photon energies above their bandgaps.³⁶ In these conditions,

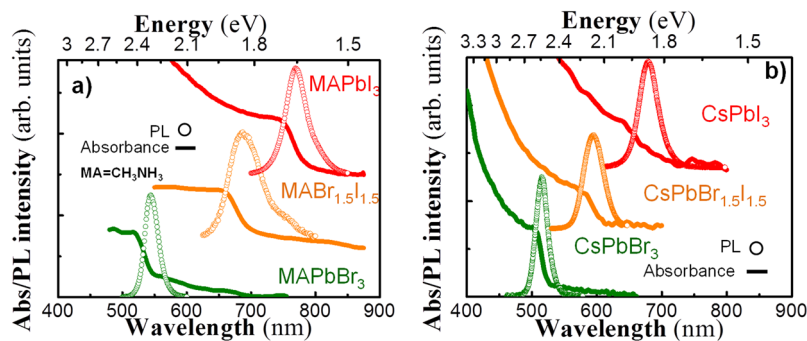


FIG. 1. Absorption (solid line) and PL (symbols) of the MHP materials used in this work. (a) Polycrystalline films of MAPbX₃. (b) CsPbX₃ NPs dispersed in a hexane solution.

TABLE I. PL properties of MAPbX₃ films and CsPbX₃ colloidal solutions.

Material	PL under 1PA			PL under 2PA, 3PA	
	E _g (eV)	PL peak (eV)	FWHM (meV)	PL peak (eV)	FWHM (meV)
MAPbBr ₃	2.40	2.41	113	2.27	90
MAPbBr _{1.5} I _{1.5}	1.87	1.88	173	1.78	125
MAPbI ₃	1.66	1.67	90	1.56	110
CsPbBr ₃	2.51	2.53	126	2.36	100
CsPbBr _{1.5} I _{1.5}	2.12	2.15	140	2.08	110
CsPbI ₃	1.88	1.85	105	1.82	100

incident light promotes the photogeneration of carriers and consequently the emission of a bright PL peak close to the band edge [symbols in Fig. 1(a)]. The overall quality of these polycrystalline films, by judging from the measured PL bandwidths, is similar to those reported in the literature.^{35,37} Here, the intensity of PL follows a linear law with excitation fluency (not shown) because each incident photon generates one electron-hole pair or it obeys a One Photon Absorption (1PA) process. It has been reported a reversible phase segregation into iodine and bromine rich phases of mixed halide perovskites under continuous illumination.⁷ This phase segregation depends on several factors such as the illumination intensity, grain size, and illumination time.³⁸ In our case, we can neglect the phase segregation effect as the ns excitation pulse is too fast to trigger this effect.

Optical properties of CsPbX₃ colloidal solutions show a similar trend and are consistent with the results published previously.³⁴ CsPbX₃ NPs exhibit a size ranged between 10 and 16 nm (see TEM images in supplementary material S1) and exhibit absorption spectra with absorption band edges located at 2.45–2.51, 2.07–2.12, and 1.74–1.88 eV for X₃ = Br₃, X₃ = Br_{1.5}I_{1.5}, and X = I₃, respectively

[solid lines in Fig. 1(b)]. In the same way, the 1PA process generates a bright PL peak close to these absorption band edges [symbols in Fig. 1(b)]. Perovskite NPs are not just interesting by the high PL quantum yield reported, despite the relatively easy preparation method and single core structure,³⁴ but also for their outstanding optoelectronic properties. For example, the black perovskite phase of CsPbI₃ is relatively unstable at room temperature for bulk materials; however, stable perovskite phases can be obtained in the form of NPs,³⁹ as the material studied in this work.

Both MAPbX₃ films and CsPbX₃ colloidal solutions present nonlinear absorption of infrared light. This process consists of the electronic promotion from the valence to the conduction band via virtual states induced by the simultaneous absorption of two (or more) photons [see scheme in Fig. 2(a)]. Under our laser excitation conditions (1 ns pulses at 1064 nm), the sum of two pump photons with energy 1.16 eV is high enough to promote Two Photon Absorption (2PA) processes in Br–I (bandgap at 1.87–2.12 eV) and I MHP families (bandgap 1.66–1.88 eV). This is not the case of Br MHP families (2.40–2.51 eV) where the laser excitation imposes a three photon absorption process (3PA) to observe the nonlinear absorption in this material. The PL derived from the multiphoton excitation is plotted in Figs. 2(b) and 2(c) for MAPbX₃ films and CsPbX₃ colloidal solutions, respectively. This is a direct proof of the existence of efficient 2PA and 3PA processes in our perovskite materials.

In comparison to emission spectra obtained under 1PA excitation, multi-photon excited PL shows narrower and red-shifted peaks (see Table I). This behavior is consistent with the results presented with films of CsPbBr₃ NPs,^{30,31} MAPbBr₃ microplates,⁴⁰ or CsPbBr₃ in colloidal solution⁴¹ and is usually explained by an enhanced self-absorption of emitted light under infrared illumination.⁴² Since the lower absorption losses of infrared light result in deeper penetration depths or even a practically uniform illumination, the PL is dominated by the longer wavelengths, presenting the lowest overlap with the absorption spectra.

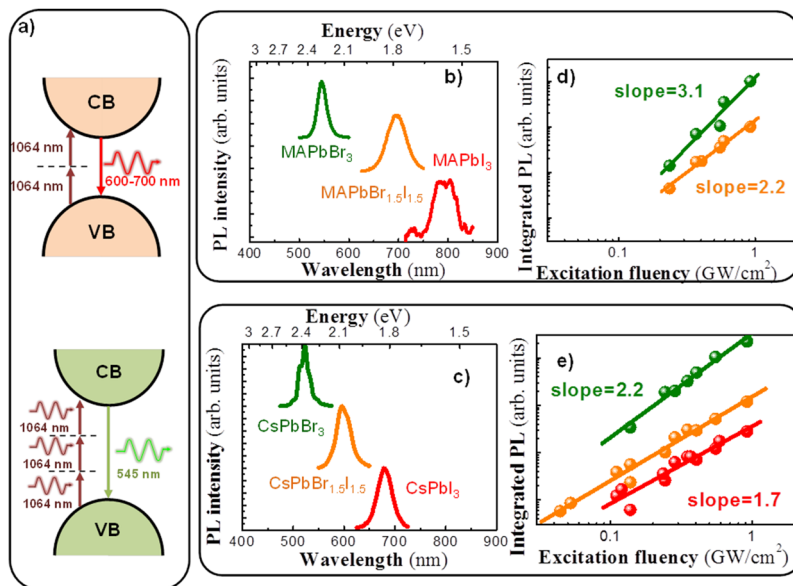
**FIG. 2.** (a) Scheme of the two photon and three photon absorption processes. PL spectra were excited at 1064 nm in (b) MAPbX₃ films and (c) CsPbX₃ NPs. Integrated PL as a function of the excitation fluency in double logarithmic scale in (d) MAPbX₃ films and (e) CsPbX₃ NPs.

TABLE II. Nonlinear parameters of MAPbX₃ films and CsPbX₃ colloidal solutions.

Material	Nonlinear absorption			Nonlinear refraction		
	Composition	E _g (eV)	β ₀	I _{sat} (GW/cm ²)	n ₂ (cm ² /GW)	FOM
MPbBr ₃	2.40	0–300 cm ³ /GW ²	1.1–3.5	...
MPbBr _{1.5} I _{1.5}	1.87	410–430 cm/GW	0.8–1.5	17.5–34.3
MPbI ₃	1.66	1100–1500 cm/GW	−[0.2–0.3]	1.25–2.5
CsPbBr ₃	2.51	0.6–1.1 cm ³ /GW ²	0.8–1	...	0.8–1.2 × 10 ^{−3}	...
CsPbBr _{1.5} I _{1.5}	2.12	0.5–0.7 cm/GW	0.6–1	...	2.5 × 10 ^{−3}	33.5–47
CsPbI ₃	1.88	0.3–0.5 cm/GW	0.3–0.8 × 10 ^{−3}	5.6–25

The dependence of the PL intensity (I_{PL}) as a function of the excitation fluency (I_0) in MAPbX₃ films corroborates the expected 2PA and 3PA excitations. Indeed, integrated PL shows a quadratic ($I_{PL} \propto I_0^{2.2}$) and cubic law ($I_{PL} \propto I_0^{3.1}$) with the excitation fluency [see Fig. 2(d)] for Br–I (orange) and Br (green) compositions, respectively. Signal to noise ratio in MPbI₃ films (red) was, however, much lower in this material, and PL under 2PA was only obtained under the highest excitation. On the other hand, I_{PL} as a function of I_0 in CsPbX₃ colloidal solutions [see Fig. 2(e)] present $I_{PL} \propto I_0^{1.7}$, $I_{PL} \propto I_0^{1.7}$, and $I_{PL} \propto I_0^{2.2}$ dependences in I, Br–I, and Br compositions, respectively. Here, the lower exponents as compared with MAPbX₃ films are attributed to self-absorption effects along the 1 mm length cuvette, resulting in a relatively important saturation of 2PA and 3PA generated PL.⁴³

Nonlinear absorption coefficient (β_2) in the different samples (see Table II) was determined by studying the transmittance of the ns-pulsed laser beam at 1064 nm as a function of the excitation fluency (I). For this purpose, a reference sample (either a borosilicate substrate or a cuvette filled with hexane to undertake the measurements on films or colloidal dispersions of NPs, respectively) was previously measured to discard artifacts in the measurement [see dashed black line in Figs. 3(a) and 3(b)]. In the case of 2PA and by considering negligible linear absorption losses at the excitation wavelength and short path lengths, the light intensity (I) traversing the sample satisfies the equation $dI/dz = -\beta_2 \cdot I^2$ and hence the transmittance through the sample results⁴⁴

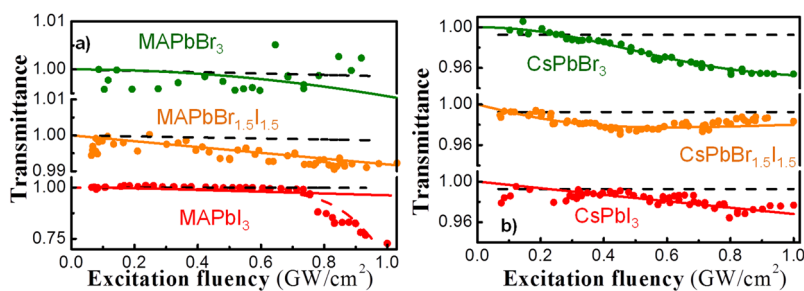
$$T = \frac{1}{1 + \beta_2 \cdot I \cdot L}, \quad (3)$$

where L is the propagation length. In the case of 3PA, the intensity of light obeys the $dI/dz = -\beta_3 \cdot I^3$ equation, and the transmittance

through the sample is⁴⁴

$$T = \frac{1}{\sqrt{1 + 2 \cdot \beta_3 \cdot I^2 \cdot L}}. \quad (4)$$

In these conditions, transmittance of MAPbI_{1.5}Br_{1.5} films [orange symbols in Fig. 3(a)] is nicely fitted [orange solid line in Fig. 2(d)] with $\beta_2 = 410\text{--}430$ cm/GW in Eq. (3). In the same way, transmittance through MAPbI₃ films [red symbols in Fig. 3(a)] shows a similar trend for excitation fluencies up to 0.7 GW/cm². Indeed, experimental values can be fitted with $\beta_2 = 1100\text{--}1500$ cm/GW (red solid line) in agreement with the E_g^{-3} scale. However, values of β_2 reported in the literature for MAPbI₃ thin films under infrared ps or fs excitation are ranging between -4.6×10^5 and 2.7×10^5 cm/GW.^{22–24} In these studies, β_2 values were obtained by the Z-scan technique, where scattering effects can overestimate the nonlinear parameters or the high intensity pulses can modify (morphology, composition) or even deteriorate the sample. In fact, for excitation fluencies higher than 0.7 GW/cm², our MAPbI₃ films present a dramatic decrease that was phenomenologically fitted by $T = 1/(10^3 \cdot I \cdot L + 26 \times 10^3 \cdot I^{10} \cdot L)$ (dashed red line) and could be explained by chemical changes under such high excitation fluencies⁴⁵ and the consequent degradation of the film.⁴⁶ On the other hand, similar characterization on MAPbI₃ quasi 2D films reported $\beta_2 \approx 23\text{--}46$ cm/GW under ps excitation.²⁸ Since these results also agree with the E_g^{-3} scale, we believe that the use of 30-fold longer excitation pulses (1 ns vs 30 ps) accounts for the higher β_2 value reported here, in agreement with the linear increase in both n_2 and β_2 parameters with the pulse width reported elsewhere.⁴⁷ Finally, the transmittance along MAPbBr₃ films [green symbols in Fig. 3(a)] practically overlaps the measurement carried out with the reference sample [open symbols in Fig. 3(a)],

**FIG. 3.** Transmittance at 1064 nm through the different samples as a function of the excitation fluency. Filled symbols and solid lines correspond to the experimental data and the fitting, respectively. (a) MAPbX₃ films and (b) CsPbX₃ NPs.

and hence, no conclusions can be extracted. Indeed, experimental data can only be fitted with smaller values of β_3 (0–300 cm³/GW²) in Eq. (4).

Similarly, experimental data of CsPbX₃ colloidal solutions can be nicely fitted with Eqs. (3) and (4), as illustrated in Fig. 3(b). Experimental transmittance on CsPbI₃ colloidal NPs [red symbols in Fig. 3(b)] obeys Eq. (5) with $\beta_2 = 0.3\text{--}0.5$ cm/GW (red solid line). In the case of transmittance through CsPbBr_{1.5}I_{1.5} NPs [orange symbols in Fig. 3(b)], a saturation of the nonlinear absorption is observed, and the following dependence of β_2 on I needs to be included:⁴⁴

$$\beta_2 = \frac{\beta_0}{1 + (I/I_{\text{sat}})^2}, \quad (5)$$

where β_0 is the nonlinear absorption without saturation and I_{sat} is a saturation intensity. In these conditions, the best fitting is obtained with $\beta_0 = 0.5\text{--}0.7$ cm/GW and $I_{\text{sat}} = 0.6\text{--}1$ GW/cm² to reproduce the experimental results (orange solid line). In this way, under the highest excitation fluency (1 GW/cm²), β_2 is reduced down to 0.25–0.35 cm/GW, in agreement with the E_g^{-3} scale. Reported results under fs excitation indicated $\beta_2 = 1.54 \times 10^{-2}$ cm/GW and $\beta_2 = 5.5 \times 10^{-2}$ cm/GW and for CsPbI₃ NPs excited at 787 nm²¹ and CsPbBr_{1.5}I_{1.5} NPs excited at 1030 nm,⁴⁸ respectively. Here, the higher values of β_2 can be explained not only by the longer excitation pulses but also by the different excitation energies (in the case of CsPbI₃) or the different concentration of NPs in the colloidal solution. Indeed, we believe that the strong difference between β_2 values reported in films and nanocrystals is due to the low concentration of NPs in the colloidal solution (filling factor around 10⁻³).²⁶

Finally, the experimental transmittance of CsPbBr₃ NPs can be well simulated with the following saturation law in the nonlinear absorption:⁴⁴

$$\beta_3 = \frac{\beta_0}{1 + (I/I_{\text{sat}})^3}, \quad (6)$$

being the best fitting parameters $\beta_0 = 0.6\text{--}1.1$ cm³/GW² and $I_{\text{sat}} = 0.8\text{--}1$ GW/cm². Here, although nonlinear absorption in Br families has been extensively characterized by the 2PA process (for example, $\beta_2 = 5\text{--}13$ and $3\text{--}9.7 \times 10^{-2}$ cm/GW are reported for monocrystals²⁷ and NPs in solution,²⁰ respectively), there are few studies where β_3 associated with a 3PA process is studied,^{49–52} given that 2PA is forbidden at long excitation wavelengths according to selection rules.⁵¹ In particular, $\beta_3 = 2.26 \times 10^{-5}$ cm³/GW² was measured in MAPbBr₃ microplates under fs excitation,^{49,50} and $\beta_3 = 0.1$ cm³/GW² was obtained in CsPbBr₃ nanoparticles under ps pulses.⁵² Again, the difference among reported values in this work and others in the literature is attributed to wider pulses of the excitation laser.

In order to complete the characterization of the nonlinear parameters on MPbX₃ films and CsPbX₃ NPs, a modification of the Z-scan technique was developed to provide an accurate determination of the nonlinear refractive index (n_2). The Z-scan setup initially proposed by Sheik-Bahae *et al.*¹⁷ consists of the translation of the nonlinear media along a Gaussian beam ($w(z)$) which is progressively focused and defocused. In these conditions, n_2 can be obtained by studying the transmittance as a function of the position of the sample (Z) through a finite aperture. By using this experimental setup as starting point, different modifications have been proposed to improve accuracy or signal to noise ratio such as reflective Z-scan⁵³ or time resolved Z-scan.⁵⁴ Here, we are interested to combine the Z-scan method with an image system.⁵⁵ For this purpose, the photodetector used in the standard Z-scan setup is replaced by a CCD camera, and a long focal lens is included between the CCD and the sample to match the far field image on the pixels of the camera [see Fig. 4(a)]. In these conditions, the optical nonlinearity can be studied by analyzing the shape of the beam, and scattering contributions can be determined and neglected. This is particularly interesting to analyze thin polycrystalline films, such as the MHP layers studied here.

First of all, the polycrystalline nature leads to strong scattering or other non-desirable effects and, consequently, can lead to

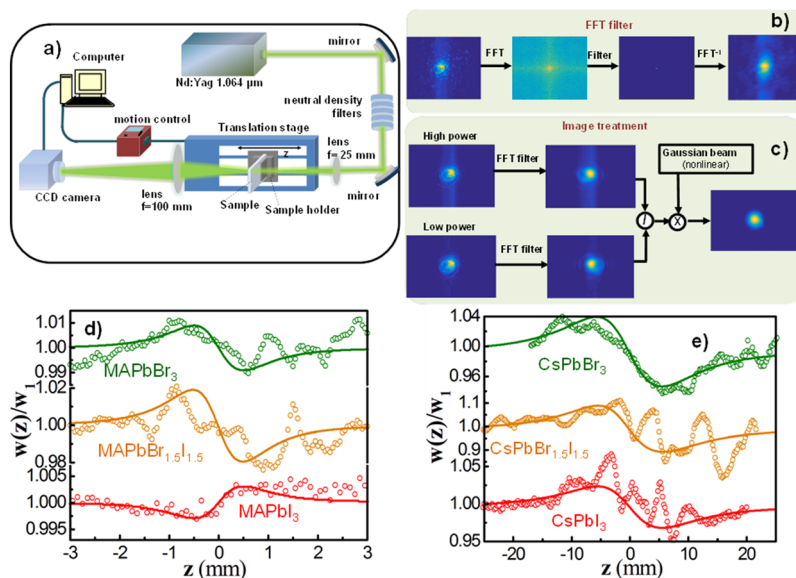


FIG. 4. (a) Z-scan experimental setup. (b) Procedure to filter nonlinear contributions. (c) Z-scan measurements based on the analysis of the image of the beam. (d) MAPbX₃ films and (e) CsPbX₃ NPs.

inaccurate and overestimated nonlinear parameters deduced by Z-scan. In addition, the high illumination fluencies required to observe nonlinearities in thin films can result in the degradation or even destruction of the MHP layers. Indeed, reported values proposed in the literature present a strong dispersion for the same materials and excitation conditions and do not follow the expected E_g^{-4} bandgap scale law.²⁶ Using our proposed procedure, light scattering (or other undesirable contributions) of the transmitted beam can be properly filtered from the recorded images. For this purpose, a FFT transform of the image is properly performed in order to filter the non-Gaussian contributions in the Fourier plane [see Fig. 4(b)]. Finally, an inverse FFT (FFT^{-1}) provides the image without these undesired contributions [see Fig. 4(b)]. Moreover, since the particular polycrystalline morphology can cause other artefacts, such as multiple reflection or interference patterns, the procedure shown in Fig. 4(b) is also carried out in order to assure the measurement of the transmitted beam. First of all, the images are recorded under high and low illumination conditions. Since nonlinear effects are only effective under high excitation fluencies, the image recorded with light under low illumination should show a Gaussian beam with a constant waist, and hence, any modification from this ideal shape should be taken into account. Then, the FFT procedure is performed on the images recorded under both intensities. The final cleaned image is obtained by multiplying the theoretical Gaussian shape (without nonlinearities) by the ratio between both signals [see Fig. 4(c)]. This procedure provides a clean Gaussian shape where the parameter n_2 can be determined by analyzing the modification of the beam as a function of Z. The accuracy of the method is corroborated by reproducing the results obtained on a reference substrate (silicon) under similar excitations (see supplementary material S2),⁵⁶ and the improvements on the Z-scan spectra obtained on polycrystalline films can be observed in supplementary material S3 and videos. It is also worth mentioning that our image analysis nicely agrees with the transmittance of the beam in a closed aperture setup, as presented in supplementary material S4.

Representative results in MAPbX₃ films and CsPbX₃ NPs are presented in Figs. 4(d) and 4(e), respectively. In all cases, the beam is concentrated and expanded close to the focus ($z = 0$). On the one hand, the peak-valley separation is a signature of the real non-linearity and depends on n_2 , the excitation fluency, and the sample thickness (L). On the other hand, the sign of n_2 determines if the Z-scan curve follows a peak-valley ($n_2 < 0$) or valley-peak shape ($n_2 > 0$).¹⁷ Analyses of these spectra in MAPbX₃ films were carried out in more than five different regions of the sample in order to discard the inhomogeneity of polycrystalline grains, and an average of fitting parameters was obtained in these different regions to take into account dispersion of data. The excitation intensity was focused on a 11–13 μm waist to assure the thin sample approximation condition ($L \ll \text{Rayleigh distance of the beam}$) and it was limited to 0.14 GW/cm^2 to avoid the influence of the nonlinear absorption [Fig. 3(a)] and/or the sample degradation. Here, it is worth mentioning that the *in situ* observation of the shape of the beam provided by the CCD image in this method allows the immediate prevention of non-desirable effects that could alter the nonlinear parameters. For example, supplementary material S5 illustrates through the acquired CCD images how the transmitted laser beam deteriorates the sample under high excitation fluencies (1 GW/cm^2). This is the reason to limit the laser fluency below the

damage threshold in the experiments, from which we obtain n_2 in MPbBr₃, MPbBr_{1.5}I_{1.5}, and MPbI₃ ranged between 1.1–3.5 cm^2/GW , 0.8–1.5 cm^2/GW , and $-[0.2-0.3] \text{cm}^2/\text{GW}$, respectively. In CsPbX₃ NPs, a larger beam waist (36–40 μm) was defined for 1 mm length cuvettes, and the experiments were carried out at a maximum power of 85 MW/cm^2 . In this way, n_2 in CsPbBr₃, CsPbBr_{1.5}I_{1.5}, and CsPbI₃ ranged between $[0.8-1.2] \times 10^{-3}$, 2.5×10^{-3} , and $[0.3-0.8] \times 10^{-3} \text{cm}^2/\text{GW}$, respectively. The ranges of the nonlinear optical parameters reported in this work represent the dispersion in the fitting parameters of all Z-scan spectra measured in different regions of every sample.

Since there is a huge dispersion on the n_2 parameter reported in MHP materials, it is difficult to compare the results presented here with those reported in the literature and reviewed elsewhere.²⁶ Among the different publications, the most accurate values for n_2 were reported for quasi 2D films²⁸ and colloidal solutions²⁰ that were in the range $[2.88-3.12] \times 10^{-5}$ and $[4.7-6.75] \times 10^{-6} \text{cm}^2/\text{GW}$, respectively. In the first case, n_2 was indirectly deduced by the third harmonic generation,²⁸ whereas in the second case, the use of a colloidal solution should minimize scattering effects.²⁰ Again, since these parameters were obtained under ps and fs excitation, we believe that the higher values of n_2 deduced in the present work can be mostly justified because of using $\approx 100-1000$ times wider excitation pulses. In fact, it has already been noted a dependence of the nonlinear optical parameters on the pulse width and repetition rate,²⁶ whose dependence is approximately linear with the increase in the pulse width.⁴⁷ The observed difference would arise from the different contributions of optical nonlinearities under different excitation regimes.²³ At short excitation pulses (fs, ps), the nonlinearity originates from bound charge carriers, whereas for wide excitation pulses, it can appear additional contributions from free carriers and/or thermal effects⁵⁷ besides electronic or vibrational ones.³³

Moreover, the results obtained here follow the trend given by the normalized n_2 coefficient (G)^{18,19}

$$G = 2 \cdot n_2 \cdot n_0^2 \cdot E_g^4 / K \cdot \sqrt{E_p} \quad (7)$$

where n_0 is the refractive index, E_p is usually fixed to 21 eV, a typical value for III–V semiconductors, and K is a material independent constant. Figure 5 shows experimental values of G for MAPbX₃ films and CsPbX₃ NPs, represented as a function of the excitation ratio $x = \text{photon-energy}/E_g$. According to Kramers-Kronig analysis, the dispersion curve $G(x)$ has a dependence given by^{18,19}

$$G(x) = \frac{-2 + 6 \cdot x - 3 \cdot x^2 - x^3 - 0.75 \cdot x^4 - 0.75 \cdot x^5 + 2 \cdot (1 - 2 \cdot x)^{1.5} \cdot H}{64 \cdot x^6}, \quad (8)$$

where H is the unit step function. Clearly, although this formula is obtained from a band-to-band model (bound electrons), our experimental data follow quite well $G(x)$, from its maximum to its change in sign. Here, n_0 is calculated from the relationship $n_0^2 = 1 + 8.32/E_g$ (eV),⁵⁸ K is fixed to 10^8 when E_g and E_p are given in eV, and n_2 for CsPbX₃ NPs was multiplied by 10^3 in order to take into account for their concentration in the colloidal solution. Again, we believe that such high K -value as compared to that used in some other studies ($K = 3100$)¹⁸ can be due to the wider pulses of the excitation laser used here.

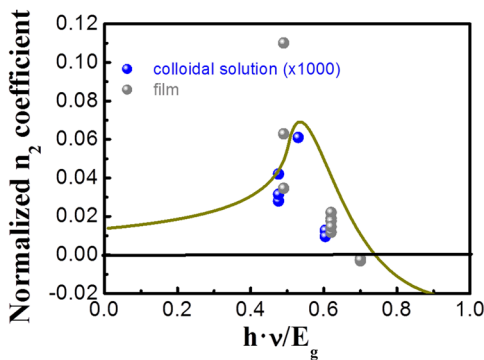


FIG. 5. Normalized n_2 coefficient, G , obtained experimentally for MAPbX₃ films and CsPbX₃ NPs, gray and blue symbols, respectively, together with the theoretical curve, solid gold line, represented by Eq. (8).

The β and n_2 coefficients obtained here under ns excitation (Table II) can be compared with reported values in the literature using fs/ps excitation at a similar wavelength, as summarized in Table III. According to Ref. 47, the shorter the excitation pulse the smaller the nonlinear optical parameters. There is only one discrepancy, the case of the giant and negative value of $\beta_2 = -2.25 \times 10^3$ reported in Ref. 22, which could be attributed to the influence of light scattering in their Z-scan measurements, as discussed above.

Finally, it is interesting to compare the magnitude of both nonlinear parameters via the calculation of the FOM with Eq. (2). FOM values of 1.25–2.5 and 17.9–33.5 are deduced for MPbI₃ and MPbBr_{1.5}I_{1.5} polycrystalline films (Table II), respectively. For MHP materials in the form of NPs, FOM values are consistently similar but slightly higher, 5.6–25 and 33.5–47 for CsPbI₃ and CsPbBr_{1.5}I_{1.5} NPs (Table II), respectively. Thus, it seems that nonlinear refraction applications will be benefited by using materials with higher E_g (Br–I families), while nonlinear absorption becomes more efficient for short E_g (I families). Of course, here there is a trade-off between both parameters, and a given material has to be carefully chosen for a given application.²⁶ According to our previous work,²⁶ these FOM values are higher than the values reported (or deduced from reported nonlinear optical parameters) for other semiconductors, including Si, GaAs, and InP, and also higher than those for nanocrystals (CdSe, CdTe, and InP) in colloidal solution or few-layer chalcogenides (MoX, X = S, Se, and Te). These features, together with the technological feasibilities of MHP materials, indicate that MAPbX₃ and CsPbX₃ perovskites are very appealing candidates to develop a new nonlinear photonic technology.

TABLE III. Results obtained with other excitation pulses at the similar wavelengths.

Material	Pulse	β_2 (cm/GW)	n_2 (cm ² /GW)	Reference
CH ₃ NH ₃ PbBr ₃	30 ps, 50 Hz	9		59
CH ₃ NH ₃ PbI ₃	30 ps, 50 Hz	23	1.37×10^{-5}	59
CH ₃ NH ₃ PbI ₃	40 ps	-2.25×10^3	3.74×10^{-2}	22
CsPb(BrI) ₃	340 fs, 1 kHz	5.5×10^{-2}		48

In this work, the nonlinear optical properties of MAPbX₃ polycrystalline thin films and CsPbX₃ nanoparticles (X₃ = I₃, Br₃, and Br_{1.5}I_{1.5}), in the latter case both in colloidal solution and forming thin films with them, were carefully studied under ns-excitation. First of all, we demonstrated the high efficiency of nonlinear absorption of infrared light in these materials because of the relatively intense generation of photoluminescence under 2PA or 3PA processes (under 1064 nm pulsed laser excitation). The transmittance technique is the most suited method to obtain the nonlinear absorption coefficient of the studied perovskites with higher accuracy than in Z-scan experiments. Values found for β in the present work for both films and NPs (taking into account their filling factor or concentration in the colloidal solution) are in the range 100–1000 cm/GW and follows the expected E_g^{-3} dependence expressed by Eq. (8). Finally, a modified Z-scan method was developed to characterize the n_2 parameter in thin polycrystalline films without the influence of light scattering. This method consists of analyzing the image of transmitted light (1 ns-pulsed laser at 1064 nm) in order to study the effects of the nonlinearity of the material on the shape of the beam. For this purpose, the non-Gaussian contributions are previously filtered, and light under high and low excitation conditions is carefully compared. This new experimental setup can be useful to analyze any polycrystalline material thin film. In particular, n_2 follows the dispersion curve $G(x)$ deduced by a two-band model and yield n_2 values up to 3.5 cm²/GW, which is one order of magnitude higher than that obtained in silicon (see supplementary material S2) or other direct bandgap semiconductors. These results indicate that both halide perovskite thin films and nanoparticle materials present a high potentiality for the development of future nonlinear optic devices.

See supplementary material for the TEM images of the nanoparticles, Z-scan analysis of silicon samples, the effect of the FFT filtering, and images of the damage monitoring. In addition, two supplementary videos show the Z-scan images before and after the FFT filtering.

Financial support from Spanish MINECO through Project No. TEC2017-86102-C2-1-R and the European Research Council (ERC) via Consolidator Grant (724424—No-LIMIT) are gratefully acknowledged. M.V.-P. acknowledges Universitat Jaume I for the support through the FPI Fellowship Program (PREDOC/2017/40).

REFERENCES

- M. V. Kovalenko, L. Protesescu, and M. I. Bodnarchuk, *Science* **358**, 745 (2017).
- T. P. White, E. Deleporte, and T.-C. Sum, *Opt. Express* **26**, A153 (2018).
- W. Mao, J. Zheng, Y. Zhang, A. S. R. Chesman, Q. Ou, J. Hicks, F. Li, Z. Wang, B. Graystone, T. D. M. Bell, M. U. Rothmann, N. W. Duffy, L. Spiccia, Y. B. Cheng, Q. Bao, and U. Bach, *Angew. Chem., Int. Ed.* **56**, 12486 (2017).
- C. C. Stoumpos, C. D. Malliakas, and M. G. Kanatzidis, *Inorg. Chem.* **52**, 9019 (2013).
- Q. A. Akkerman, G. Rainò, M. V. Kovalenko, and L. Manna, *Nat. Mater.* **17**, 394 (2018).
- Q. A. Akkerman, A. L. Abdelhady, and L. Manna, *J. Phys. Chem. Lett.* **9**, 2326 (2018).
- W. S. Yang, B. W. Park, E. H. Jung, N. J. Jeon, Y. C. Kim, D. U. Lee, S. S. Shin, J. Seo, E. K. Kim, J. H. Noh, and S. I. Seok, *Science* **356**, 1376 (2017).
- B. R. Sutherland and E. H. Sargent, *Nat. Photonics* **10**, 295 (2016).

- ⁹I. Suárez Alvarez, *Eur. Phys. J.: Appl. Phys.* **75**, 30001 (2016).
- ¹⁰T. T. Ngo, I. Suarez, G. Antonicelli, D. Cortizo-Lacalle, J. P. Martinez-Pastor, A. Mateo-Alonso, and I. Mora-Sero, *Adv. Mater.* **29**, 1604056 (2017).
- ¹¹I. Suárez, E. J. Juárez-Pérez, J. Bisquert, I. Mora-Seró, and J. P. Martínez-Pastor, *Adv. Mater.* **27**, 6157 (2015).
- ¹²H. Zhu, Y. Fu, F. Meng, X. Wu, Z. Gong, Q. Ding, M. V. Gustafsson, M. T. Trinh, S. Jin, and X.-Y. Zhu, *Nat. Mater.* **14**, 636 (2015).
- ¹³I. Suárez, E. Hassanabadi, A. Maulu, N. Carlino, C. A. Maestri, M. Latifi, P. Bettotti, I. Mora-Seró, and J. P. Martínez-Pastor, *Adv. Opt. Mater.* **6**, 1800201 (2018).
- ¹⁴N. Pourdavoud, S. Wang, A. Mayer, T. Hu, Y. Chen, A. Marianovich, W. Kowalsky, R. Heiderhoff, H. C. Scheer, and T. Riedl, *Adv. Mater.* **29**, 1 (2017).
- ¹⁵R. W. Boyd, *Nonlinear Optics*, 3rd ed. (Elsevier, Rochester, New York, 2007).
- ¹⁶J. Leuthold, C. Koos, and W. Freude, *Nat. Photonics* **4**, 535 (2010).
- ¹⁷M. Sheik-Bahae, A. A. Said, T.-H. Wei, D. J. Hagan, and E. W. Van Stryland, *IEEE J. Quantum Electron.* **26**, 760 (1990).
- ¹⁸M. Sheik-Bahae, D. C. D. Hutchings, D. J. Hagan, and E. W. Van Stryland, *IEEE J. Sel. Top. Quantum Electron.* **27**, 1296 (1991).
- ¹⁹M. Sheik-Bahae, D. J. Hagan, and E. W. Van Stryland, *Phys. Rev. Lett.* **65**, 96 (1990).
- ²⁰W.-G. Lu, C. Chen, D. Han, L. Yao, J. Han, H. Zhong, and Y. Wang, *Adv. Opt. Mater.* **4**, 1732 (2016).
- ²¹S. Liu, G. Chen, Y. Huang, S. Lin, Y. Zhang, M. He, W. Xiang, and X. Liang, *J. Alloys Compd.* **724**, 889 (2017).
- ²²R. Zhang, J. Fan, X. Zhang, H. Yu, H. Zhang, Y. Mai, T. Xu, J. Wang, and H. J. Snaith, *ACS Photonics* **3**, 371 (2016).
- ²³B. S. Kalanoor, L. Gouda, R. Gottesman, S. Tirosh, E. Haltzi, A. Zaban, and Y. R. Tischler, *ACS Photonics* **3**, 361 (2016).
- ²⁴J. Y. I. Un, L. I. L. I. M. Iao, J. L. I. Ie, W. H. U. Ei, C. H. Z. Hao, and S. H. W. En, *Opt. Mater. Express* **7**, 3894 (2017).
- ²⁵K. N. Krishnakanth, S. Seth, A. Samanta, and S. V. Rao, *Opt. Lett.* **43**, 603 (2018).
- ²⁶A. Ferrando, J. P. M. Pastor, and I. Suárez, *J. Phys. Chem. Lett.* **9**, 5612 (2018).
- ²⁷G. Walters, B. R. Sutherland, S. Hoogland, D. Shi, R. Comin, D. P. Sellan, O. M. Bakr, and E. H. Sargent, *ACS Nano* **9**, 9340 (2015).
- ²⁸F. O. Saouma, C. C. Stoumpos, J. Wong, M. G. Kanatzidis, and J. I. Jang, *Nat. Commun.* **8**, 742 (2017).
- ²⁹W. Liu, J. Xing, J. Zhao, X. Wen, K. Wang, P. Lu, and Q. Xiong, *Adv. Opt. Mater.* **5**, 1601045 (2017).
- ³⁰Y. Xu, Q. Chen, C. Zhang, R. Wang, H. Wu, X. Zhang, G. Xing, W. W. Yu, X. Wang, Y. Zhang, and M. Xiao, *J. Am. Chem. Soc.* **138**, 3761 (2016).
- ³¹Z. Hu, Z. Liu, Y. Bian, D. Liu, X. Tang, W. Hu, Z. Zang, M. Zhou, L. Sun, J. Tang, Y. Li, J. Du, and Y. Leng, *Adv. Opt. Mater.* **5**, 1700419 (2017).
- ³²G. Jiang, L. Miao, J. Yi, B. Huang, W. Peng, Y. Zou, H. Huang, W. Hu, C. Zhao, and S. Wen, *Appl. Phys. Lett.* **110**, 161111 (2017).
- ³³R. Adair, L. Chase, and S. A. Payne, *Phys. Rev. B* **39**, 3337 (1989).
- ³⁴L. Protesescu, S. Yakunin, M. I. Bodnarchuk, F. Krieg, R. Caputo, C. H. Hendon, R. X. Yang, A. Walsh, and M. V. Kovalenko, *Nano Lett.* **15**, 3692 (2015).
- ³⁵A. Sadhanala, F. Deschler, T. H. Thomas, S. E. Dutton, K. C. Goedel, F. C. Hanusch, M. L. Lai, U. Steiner, T. Bein, P. Docampo, D. Cahen, and R. H. Friend, *J. Phys. Chem. Lett.* **5**, 2501 (2014).
- ³⁶S. De Wolf, J. Holovsky, S. J. Moon, P. Löper, B. Niesen, M. Ledinsky, F. J. Haug, J. H. Yum, and C. Ballif, *J. Phys. Chem. Lett.* **5**, 1035 (2014).
- ³⁷S. Draguta, S. Thakur, Y. V. Morozov, Y. Wang, J. S. Manser, P. V. Kamat, and M. Kuno, *J. Phys. Chem. Lett.* **7**, 715 (2016).
- ³⁸A. F. Gualdrón-Reyes, S. J. Yoon, and I. Mora-Seró, *Curr. Opin. Electrochem.* **11**, 84 (2018).
- ³⁹A. Swarnkar, A. R. Marshall, E. M. Sanehira, B. D. Chernomordik, D. T. Moore, J. A. Christians, T. Chakrabarti, and J. M. Luther, *Science* **354**, 92 (2016).
- ⁴⁰Q. Wei, B. Du, B. Wu, J. Guo, M. jie Li, J. Fu, Z. Zhang, J. Yu, T. Hou, G. Xing, T. C. Sum, and W. Huang, *Adv. Opt. Mater.* **5**, 1700809 (2017).
- ⁴¹Y. Wang, X. Li, X. Zhao, L. Xiao, H. Zeng, and H. Sun, *Nano Lett.* **16**, 448 (2015).
- ⁴²Y. Wang, D. Yu, Z. Wang, X. Li, X. Chen, V. Nalla, H. Zeng, and H. Sun, *Small* **13**, 1701587 (2017).
- ⁴³I. Suárez, H. Gordillo, R. Abargues, S. Albert, and J. Martínez-Pastor, *Nanotechnology* **22**, 435202 (2011).
- ⁴⁴L. Tan and W. A. F. Base, *Chem. Rev.* **108**, 1245 (2008).
- ⁴⁵P. K. Kanaujia and G. Vijaya Prakash, *Phys. Chem. Chem. Phys.* **18**, 9666 (2016).
- ⁴⁶Z. Ahmad, M. A. Najeed, R. A. Shakoor, A. Alashraf, S. A. Al-Muhtaseb, A. Soliman, and M. K. Nazeeruddin, *Sci. Rep.* **7**, 15406 (2017).
- ⁴⁷K. Shinkawa and K. Ogusu, *Opt. Express* **16**, 18230 (2008).
- ⁴⁸J. Li, S. Zhang, H. Dong, X. Yuan, X. Jiang, J. Wang, and L. Zhang, *CrystEngComm* **18**, 7945 (2016).
- ⁴⁹G. Weng, J. Xue, J. Tian, X. Hu, X. Bao, H. Lin, S. Chen, Z. Zhu, and J. Chu, *ACS Photonics* **5**, 2951 (2018).
- ⁵⁰Y. Gao, S. Wang, C. Huang, N. Yi, K. Wang, S. Xiao, and Q. Song, *Sci. Rep.* **7**, 45391 (2017).
- ⁵¹F. O. Saouma, C. C. Stoumpos, M. G. Kanatzidis, Y. S. Kim, and J. I. Jang, *J. Phys. Chem. Lett.* **8**, 4912–4917 (2017).
- ⁵²D. J. Clark, C. C. Stoumpos, F. O. Saouma, M. G. Kanatzidis, and J. I. Jang, *Phys. Rev. B* **93**, 195202 (2016).
- ⁵³D. V. Petrov, A. S. L. Gomes, and C. B. De Araújo, *Appl. Phys. Lett.* **65**, 1067 (1994).
- ⁵⁴M. Reichert, H. Hu, M. R. Ferdinandus, M. Seidel, P. Zhao, T. R. Enslay, D. Peceli, J. M. Reed, D. A. Fishman, S. Webster, D. J. Hagan, and E. W. Van Stryland, *Optica* **1**, 436 (2014).
- ⁵⁵G. Boudebs and K. Fedus, *J. Appl. Phys.* **105**, 103106 (2009).
- ⁵⁶K. Ogusu and K. Shinkawa, *Opt. Express* **16**, 14780 (2008).
- ⁵⁷F. L. S. Cuppo, A. M. Figueiredo Neto, S. L. Gómez, and P. Palfy-Muhoray, *J. Opt. Soc. Am. B* **19**, 1342 (2002).
- ⁵⁸M. A. Green, Y. Jiang, A. M. Soufiani, and A. Ho-Baillie, *J. Phys. Chem. Lett.* **6**, 4774 (2015).
- ⁵⁹F. O. Saouma, D. Y. Park, S. H. Kim, M. S. Jeong, and J. I. Jang, *Chem. Mater.* **29**, 6876 (2017).